# Permanent Magnet Assisted Synchronous Reluctance Motor with Asymmetric Rotor for High Torque Performance

Chengwu Diao, Wenliang Zhao, *Member*, *IEEE*, Yan Liu, and Xiuhe Wang

***Abstract*— Permanent magnet assisted synchronous reluctance motor (PMA-SynRM) is a kind of high torque density energy conversion device widely used in modern industry. In this paper, based on the basic topology of PMA-SynRM, a novel PMA-SynRM of asymmetric rotor with position-biased magnet is proposed. The asymmetric rotor design with position-biased magnet realizes the concentration of magnetic field lines in the motor air gap to obtain higher electromagnetic torque, and makes both of magnetic and reluctance torque obtain the peak value at the same current phase angle. The asymmetric rotor configuration is theoretically illustrated by space vector diagram, and the feasibility of high torque performance of the motor is verified. Through the finite element simulation, the effect of the side barrier on output torque and the Mises stress under the rotor asymmetrical design are analyzed. Then the motor characteristics including airgap flux density, back EMF, magnetic torque, reluctance torque, torque ripple, losses, and efficiency are calculated for both the basic and proposed PMA-SynRMs. The results show that the proposed PMA-SynRM has higher torque and efficiency than the basic topology. Moreover, the torque ripple of the proposed PMA-SynRM is reduced by the method with harmonic current injection, and the torque characteristics in the whole current cycle are analyzed. Finally, the endurance to avoid PM demagnetization is confirmed based on the PM remanence calculation.**

***Index Terms*—Permanent magnet assisted synchronous reluctance motor, Asymmetric rotor, Magnetic torque, Reluctance torque, Torque ripple.**

## I. Introduction

As a high torque density electromagnetic energy conversion device with low cost and simple structure, the permanent magnet (PM) motor is widely applied in various applications, while its performance is directly related to the performance of permanent magnets [1]-[2]. At present, the application of high-performance PMs such as NdFeB has significantly improved the efficiency and torque/power density of PM motor [3]-[4]. However, as a non-renewable resource, NdFeB material is directly affected by market supply and resource reserves [5]-[6]. Owing to the increasing concern of the price and supply of PMs, the permanent magnet assisted synchronous reluctance motor (PMA-SynRM) has been widely promoted due to the less PM usage, high torque/power density, and wide speed range by integrating the advantages of PM and reluctance motors, [7]- [9].

The current research on performance of PMA-SynRM mainly focuses on permanent magnet design, magnetic circuit analysis and flux barrier design [10]-[11]. The torque performance of PMA-SynRM was improved by analyzing the number of PMs and PM geometry [12]-[13]. Considering the large-scale production, the processing of long arc PMs of PMA-SynRM is more complicated and difficult to install. Therefore, segmented rectangular PMs are used instead to facilitate manufacturing and assembly [14]. By optimizing the saturation of the rotor magnetic circuit, the torque of the PMA-SynRM can be further improved [15]. The size of motor is optimized according to the distribution of the rotor flux density, so as to make the most of the PM and reduce the torque ripple [16]. By adjusting the number and structure of the core flux barrier, the PMA-SynRM reluctance torque is improved and the torque ripple is reduced [17]. The role of the flux barrier has been extended from simply preventing magnetic leakage to improving the reluctance torque [18]. Arc flux barrier and U-shaped flux barrier are two widely used flux barrier structures. Among them, arc-shaped flux barrier is conducive to PMA-SynRM to obtain greater torque and power density [19], [20]. However, most of the reported PMA-SynRMs are generally designed with only partial use of the magnetic and reluctance torques. To improve the utilization of torque components, a specially designed PMA-SynRM is proposed, which can improve the utilization rate of each torque component by changing the torque relationship by adjusting the flux barrier and PM position [21]-[22]. Based on it, PMA-SynRM with asymmetric V-shape PMs and asymmetric flux barriers is proposed, and the performance are researched. The obtained asymmetric rotor structure superimposes the magnetic torque and reluctance torque components at the peak point, thereby increasing the average torque with the same amount of PMs [23]. Due to the asymmetry of the rotor caused by the adjustment, the torque ripple of the motor increases accordingly, and the output stability decreases [24]. To solve it, PMA-SynRM with a side rib in the rotor barrier is proposed. The added side rib provides a demagnetization path for the

Manuscript received August 17, 2022; revised October 08, 2022; accepted November 01, 2022. Date of publication June 25, 2023; Date of current version January 17, 2023.

This work was supported in part by the National Natural Science Foundation of China under Grant 52077123 and 51737008, and in part by the Natural Science Foundation of Shandong Province of China for Outstanding Young Scholars, under Grant ZR2021YQ35. (*Corresponding author: Wenliang Zhao*.)

C. Diao, W. Zhao, and X. Wang are with the School of Electrical Engineering, Shandong University, Jinan, 250061, China(e-mail: diaochengwu@mail.sdu.edu.cn; wlzhao@sdu.edu.cn; wangxh@sdu.edu.cn)

Y. Liu is with the China Aviation Control System Research Institute, Wuxi, 214000, China(e-mail: 502675899@qq.com).

Digital Object Identifier 10.30941/CESTEMS.2023.00016

armature winding so as to reduce the torque ripple [25]. In a word, through the configuration of the flux barriers and PM, the magnetic flux path is changed, which will reduce the current angle difference where the two torque components appear.

In this paper, a novel PMA-SynRM with an asymmetric rotor is proposed to increase the performance including torque and efficiency by focusing the magnetic flux and improving the utilization of torque components. The design principle is illustrated by space vector diagram with a theoretical analysis. The effect of the side barrier on torque of proposed PMA-SynRM and Mises stress of the rotor are first analyzed by the FEM. Then the characteristics of both basic and proposed PMA-SynRMs are analyzed and compared in detail. And a high-order harmonic current injection method is used to restrain the harmonic torque ripple of the motor. Finally, the PM demagnetization performance of the proposed model under overcurrent conditions is verified.

## II. Topology and Principleof the PMA-SynRMs

### A. The Basic and Proposed PMA-SynRMs

The basic model uses a 6-pole 27-slot PMA-SynRM with three layers of U-shaped flux barrier and PMs. The stator and rotor are superimposed by 50H470 silicon steel sheets, and the PM is NEOMAX-P6 with remanence of 0.54T. Compared with the basic model, the proposed PMA-SynRM model has the consistent stator structure and winding configuration, while its rotor has position-biased PM arrangements for flux focusing effects and asymmetric flux barrier to improve utilization of magnetic and reluctance torque. The rotor of the basic model, the asymmetric rotor of the proposed model and the topology of the stator are shown in Fig. 1. The amount of silicon steel sheet used in the two rotors is similar, and the proposed rotor can be transformed from the basic rotor by punching and shearing. It should be noted that the arrow of the proposed model shows the direction of PM magnetization direction, and the A region acts as flux interdicting effects, while the B region acts as flux focusing effects. Both two PMA-SynRM models have the same specifications as shown in Table I.

TABLE I
THE PARAMETERS OF THE PMA-SYNRMS

| Item | Unit | Conv. model | Prop. model |
|---|---|---|---|
| Pole/Slot | / | 6/27 | |
| Stator outer diameter | mm | 88 | |
| Stator inner diameter | mm | 51 | |
| Rotor outer diameter | mm | 50 | |
| Rotor inner diameter | mm | 15 | |
| Airgap length | mm | 0.5 | |
| Motor axial length | mm | 52 | |
| Remanence of magnet | T | 0.54 | |
| PM amount | g | 44 | |

### B. Torque Characteristics Analysis of Proposed PMA-SynRM

Flux linkage of the basic model is shown in Fig. 2(a). The d-axis of the basic model with symmetric rotor topology coincides with the direction of the PM flux linkage. Under the

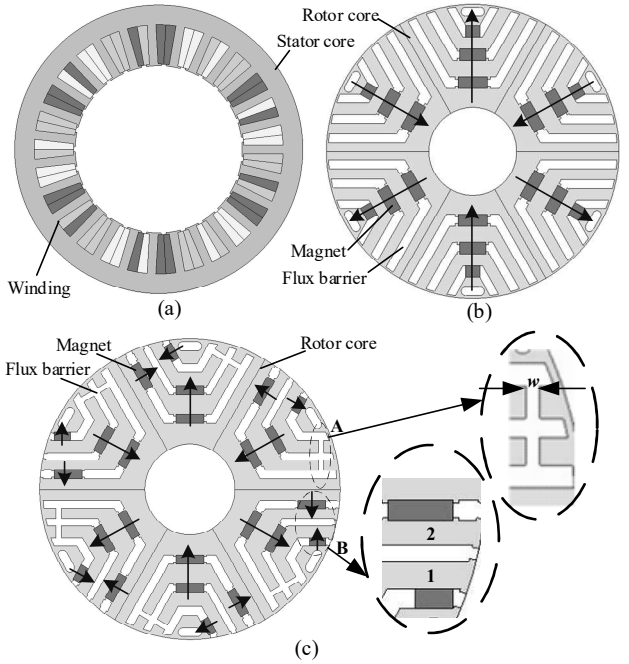


Fig. 1. The topology of PMA-SynRMs. (a) The stator and windings. (b) The basic model rotor and PMs. (c) The proposed model rotor and PMs

$dq$ coordinate axis, the motor vector diagram of the basic model is shown in Fig. 2(c). The total torque $T_{em1}$ of the basic model is obtained as:

$$T_{em1} = \frac{3p}{4}\psi_{PM} i_s \cos\theta + \frac{3p}{8}(L_d - L_q) i_s^2 \sin(2\theta) = T_{PM1} + T_{RE1} \quad (1)$$

where $p$ is the number of the poles, $\psi_{PM}$ is the flux linkage of the basic model, $i_s$ is the current vector of the PMA-SynRM stator, $L_d$ and $L_q$ are the inductance of d-axis and q-axis, respectively, and $\theta$ is the current phase angle, which is the angle between the stator current vector and the axis orthogonal to the axis of $\psi_{PM}$. The q-axis is perpendicular to the axis of $\psi_{PM}$.

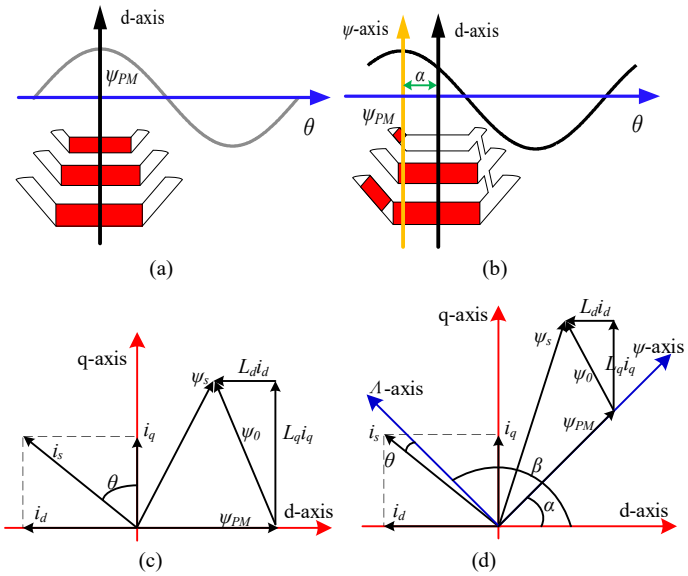


Fig. 2. Flux linkage offset and vector diagram in $dq$ axis. (a) Flux linkage of basic model. (b) Offset flux linkage of proposed model. (c) Vector diagram of basic model. (d) Offset vector diagram of proposed model.

As shown in (1), the total electromagnetic torque of the basic model consists of magnetic torque $T_{PM1}$ and reluctance torque $T_{RE1}$. $T_{PM1}$ and $T_{RE1}$ cannot reach corresponding peaks at the same time. When the current phase angle $\theta$=2nπ, $T_{PM1}$ gets the peak value, when the current phase angle $\theta$=nπ+π/4, $T_{RE1}$ gets the peak value. The current phase angles $\theta$ of the peak values of $T_{PM1}$ and $T_{RE1}$ differ by 45°, indicating that both torque components cannot simultaneously obtain their peak values in the basic designs.

As shown in Fig 2(b), in the proposed model, through the design of A and B regions, the flux linkage generated by the rotor PMs will be offset and form an angle $\alpha$=π/4 with the basic d-axis. Therefore, the vector diagram of the proposed model is different from the basic model in the $dq$ axis.

The vector diagram of the proposed model is shown in Fig. 2(d). In order to facilitate the analysis of the influence of the flux linkage offset on the motor output, the flux linkage $\psi_{PM}$ generated by the rotor PM is defined as the axis of the $\psi$ axis. And orthogonal to the $\psi$ axis is the Λ axis. The current phase angle $\theta$ is the angle between the stator current vector and the Λ axis.

In Fig. 2(d), the stator current on the d-axis and q-axis is obtained as:

$$\begin{cases} i_d = i_s \cos(\beta+\theta) \\ i_q = i_s \sin(\beta+\theta) \end{cases} \tag{2}$$

where $\beta$ is the angle between the $\Lambda$-axis and the d-axis. The flux linkage in the $\Lambda$-axis and the $\psi$-axis can be expressed as:

$$\begin{cases} \psi_d = L_d i_d + \psi_{PM} \cos\alpha \\ \psi_d = L_q i_q + \psi_{PM} \sin\alpha \end{cases} \tag{3}$$

Accordingly, the voltage on the stator $dq$ axis can be expressed as:

$$\begin{bmatrix} v_q \\ v_d \end{bmatrix} = R_a \begin{bmatrix} i_q \\ i_d \end{bmatrix} + \frac{d}{dt}\begin{bmatrix} \psi_q \\ \psi_d \end{bmatrix} + \begin{bmatrix} 0 & 1 \\ -1 & 0 \end{bmatrix}\begin{bmatrix} \psi_q \\ \psi_d \end{bmatrix} \tag{4}$$

The electromagnetic torque $T_{em2}$ of the proposed model is obtained as:

$$\begin{aligned} T_{em2} &= \frac{3p}{4}(\psi_d i_q - \psi_q i_d) \\ &= \frac{3p}{4}\psi_{PM} i_s \sin(\beta-\alpha+\theta) + \frac{3p}{8}(L_d - L_q) i_s^2 \sin 2(\beta+\theta) \\ &= T_{PM2} + T_{RE2} \end{aligned} \tag{5}$$

As shown in (5), the total torque of the proposed model consists of magnetic torque $T_{PM2}$ and reluctance torque $T_{RE2}$. And the relationship between $\alpha$ and $\beta$ can be expressed as:

$$\beta = \frac{\pi}{2} + \alpha \tag{6}$$

In the proposed model, the reluctance of the d-axis is greater than that of the q-axis. The value of $L_d$-$L_q$ is negative. When $\theta$=0, the electromagnetic torque can be expressed as:

$$T_{em2\ \theta=0} = \frac{3p}{4}\psi_{PM} i_s + \frac{3p}{8}(L_q - L_d) i_s^2 = T_{PM2\max} + T_{RE2\max} \tag{7}$$

This means that $T_{PM2}$ and $T_{RE2}$ in (7) can obtain a peak value at a certain current phase angle, thereby maximizing the use of magnetic torque and reluctance torque, and greatly improving the total torque.

## III. Analysis Result by the FEM

### A. Rotor Structure Analysis

In the proposed model rotor shown in Fig. 1(c), the flux interdicting effects in the A region are critical to realize the asymmetric rotor strategy. The side barrier which connects the three barriers on the right directly interdicts the magnet flux and affects the motor performance. Therefore, the influence of the side barrier width $w$ on the torque at different current phase angles is analyzed, as shown in Fig. 3, which shows that the width of the side barrier $w$ can sensitively affect the flux focusing effects.

As designed, under the effects of the A and B regions, the total torque of the motor obtains the peak value when the current phase angle is 0 degree except for the case of $w$ = 0.5 mm, and the largest torque is obtained at $w$ = 1.1 mm.

To verify the reliability of the asymmetric rotor structure, the rotor Mises stress caused by centrifugal force is analyzed for both models. The Mises stress results of the two models at 2000 rpm are shown in Fig. 4. The maximum Mises stress of the basic rotor is 17.89 MPa, while the maximum stress of the proposed rotor is 22.07 MPa. The maximum Mises stress value of the proposed model with different widths of the side barrier $w$ at different speeds is shown in Fig. 5. With reference to the steel material data sheet and the stress analysis of the relevant motor design, the results confirm that the proposed model is reliable during the operation [14], [26].

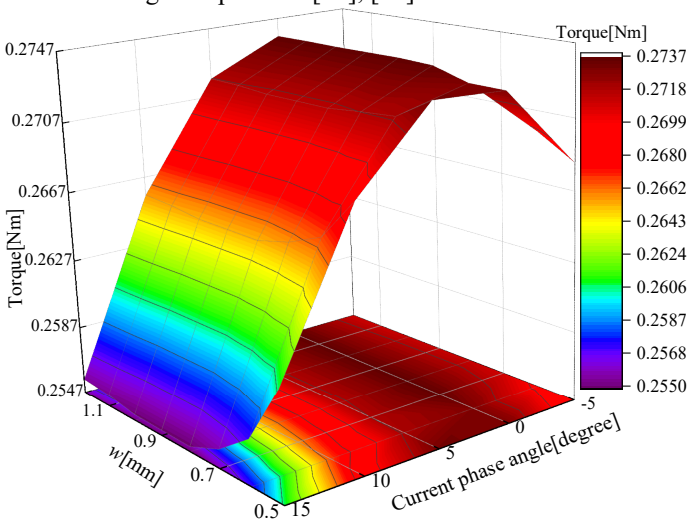


Fig. 3. The torque of the prop. model versus the $w$ and current phase angle.

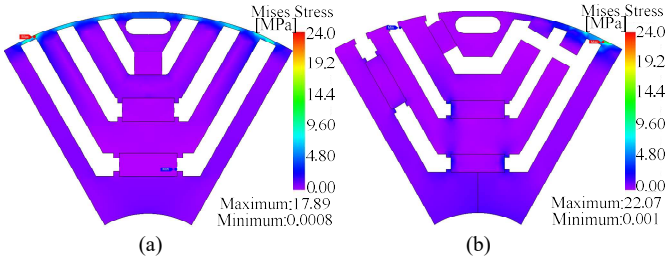


(a) (b)

Fig. 4. The contour plot of Mises stress. (a) Basic model. (b) Prop. model with $w$=1.1mm.

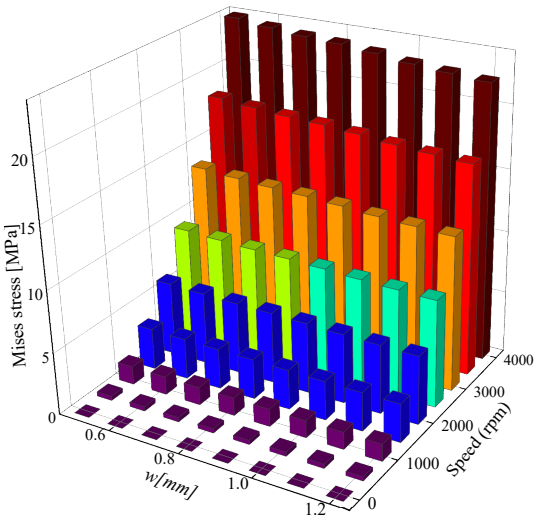


Fig. 5. The Mises stress versus $w$ and speed of the prop. model.

### B. *No-load Characteristics Analysis*

To further reveal the principle of flux focusing effects, the comparative analysis of no-load operation was carried out between the basic and the proposed model.

Fig. 6 shows the distribution of magnetic flux lines under no-load conditions for the two models. In Fig. 6(a), the magnetic flux lines of the basic model are symmetrically and evenly distributed. In Fig. 6(b), due to the flux offset design, the magnetic flux lines are asymmetrical in distribution. And the flux lines in region B are denser as flux focusing effect while most of them enter the stator core through paths 1 and 2.

Therefore, the airgap magnetic density of the proposed model is relatively improved with two protrusions when compared with the basic model, as shown in Fig. 7. Due to the

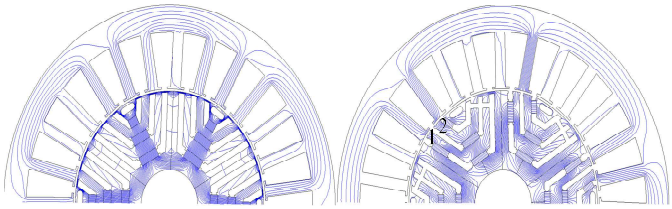


(a) (b)

Fig. 6. Magnetic flux line distributions at the no-load case. (a) Basic model. (b) Prop. model.

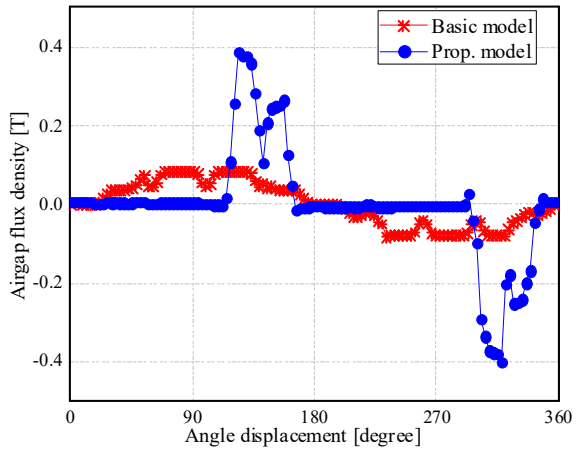


Fig. 7. Comparison of air gap flux density under no-load condition.

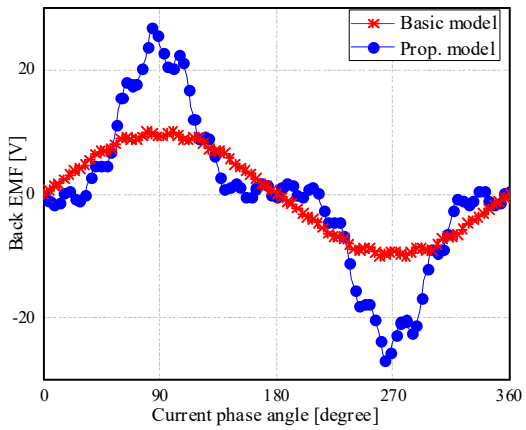


Fig. 8. Back EMF of basic model and prop. model over a period.

flux focusing effects of the asymmetric rotor, the back EMF of the proposed model has a larger amplitude than that of the basic model as shown in Fig. 8. The RMS value of the proposed model is increase by 1.8 times higher than that of the basic model.

### C. *On-load Characteristics Analysis*

The torque characteristics about reluctance and magnetic torque of both models are shown in Fig. 9 at stator current density of 3.2 Arms/mm$^2$. Due to the nonlinearity of ferromagnetic materials, the model electromagnetic torque is divided into magnetic torque and reluctance torque by using the frozen permeability method. The result shows that the peak values of the magnetic torque and reluctance torque in the basic model are obtained and its current phase angle is different, while the magnetic torque and reluctance torque of the proposed model both reach the maximum when the current phase angle is 0 degree, which is consistent with the theoretical analysis.

Compared with the basic model of symmetric rotor, the proposed model significantly improves the magnetic torque due to the magnetic flux focusing effect in the B region, but reduces the reluctance torque due to the magnetic flux interdicting effect in the A region. Fig. 10 shows the magnetic flux density distribution of the two models under the peak torque. Compared with the basic model, the proposed model has a higher overall magnetic flux density, which reveals that the proposed model has higher rotor magnetic circuit utilization.

The motor performance parameters of both models are shown in Table II. It is proposed that the back electromotive force (EMF) of the model is significantly increased due to the

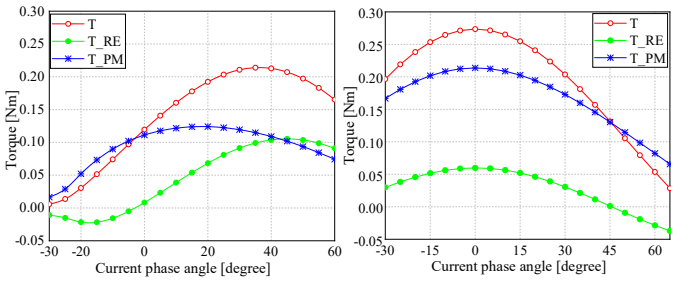


(a) (b)

Fig. 9. Torque characteristics of the two models. T: electromagnetic torque, T_RE: reluctance torque, T_PM: magnetic torque. (a) Basic model. (b) Prop. model.

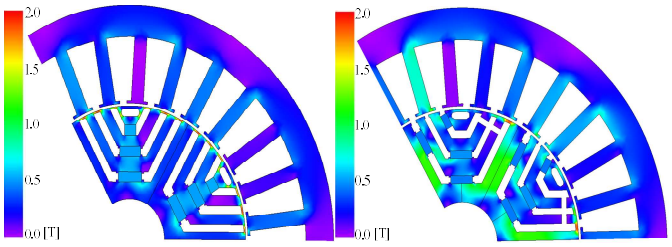


Fig. 10. Magnetic flux density at peak torque. (a) Basic model. (b) Prop. model.

flux focusing effect, and the output power is also increased accordingly. The proposed model is only improved on rotor structure, so the total loss of the motor is relatively unchanged. Compared to the basic model, the proposed model has a 28.04% increase in total torque and around 0.85% increase in efficiency at 2000rpm. The output torque of the proposed model has been effectively improved, but there is also the problem of increased torque ripple that needs further analysis.

Fig. 11 shows the electromagnetic torque of both models under the condition of peak torque. It can be seen from the Fig .11 that the electromagnetic torque of the proposed model is larger than the basic model, and the torque ripple is also higher than that of the basic model, as shown in Table II.

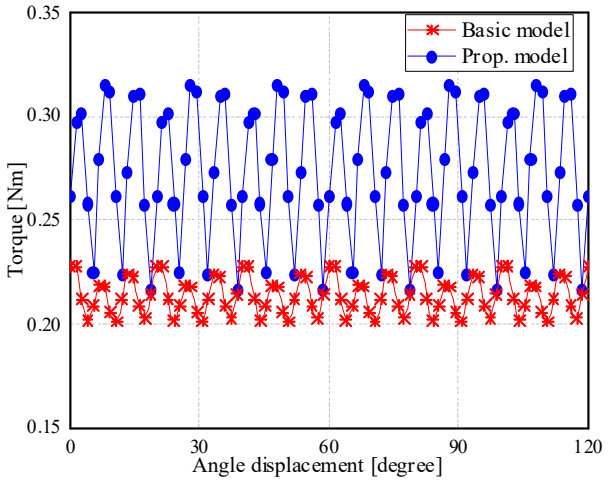


Fig. 11. Electromagnetic torques of both model at peak value.

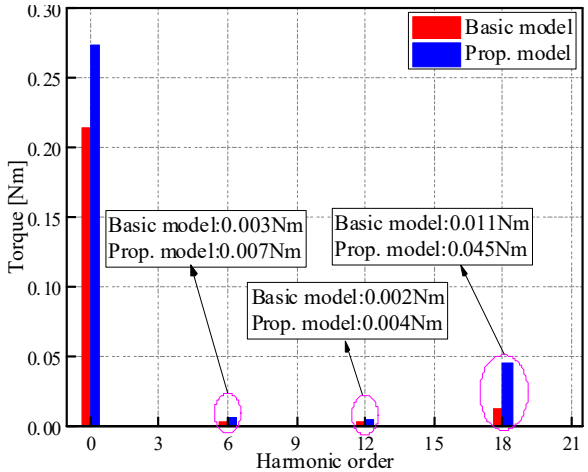


Fig. 12. Electromagnetic torque harmonic analysis and comparison.

TABLE II
COMPARISON OF THE OUTPUT PERFORMANCE OF BOTH MODELS

| Item | Unit | Conv. model | Prop. model |
|---|---|---|---|
| EMF(RMS) | V | 6.79 | 12.27 |
| Torque | Nm | 0.214 | 0.274 |
| Torque ripple | % | 12.5% | 35.9% |
| Power | W | 49.94 | 63.12 |
| Total loss | W | 4.98 | 5.81 |
| Efficiency | % | 90.02 | 90.80 |

In order to further analyze the causes of the increase of torque ripple, the harmonic analysis of motor torque is carried out. The result of the torque harmonic analysis is shown in Fig.12, which shows that the dominant 6th, 12th, and 18th harmonic torques of the proposed model are increased. And through harmonic analysis of the proposed model, it is found that the high torque ripple is mainly caused by the added 18th harmonic component. On the premise of ensuring the maximum utilization of the proposed model's permanent magnet torque and reluctance torque, the method of harmonic current injection is used to reduce the torque ripple so as to ensure electromagnetic performance without destroying the electromagnetic structure [27].

The principle of harmonic current injection is shown in Fig. 13. The 17th and 19th harmonic currents are injected into the current excitation to generate the harmonic compensation voltage and magnetomotive force, which are used to generate a new 18th torque harmonic component to offset the original 18th torque harmonic component. To counteract torque ripple, the harmonic current to be injected is:

$$I_{Inject} = I_{17}\sin(17\omega t + \varphi_{17}) + I_{19}\sin(19\omega t + \varphi_{19}) \tag{8}$$

where $I_{17}$ and $I_{19}$ are the 17th and 19th harmonic current, respectively, $\omega$ is the angular velocity of the model, and $\varphi_{17}$ and $\varphi_{19}$ are the initial phase angle of the 17th harmonic current and 19th harmonic current, respectively.

Among them, $I_{17}$ and $I_{19}$ can be obtained by (9), $\varphi_{17}$ and $\varphi_{19}$ can be obtained by (10).

$$I_N = -\frac{E_N}{E_1} \times I_1 \tag{9}$$

$$\varphi_N = \frac{\pi}{2} + \varphi_{EN} \tag{10}$$

where $N$ is the harmonic order, $E$ and $I$ are the amplitude of the back EMF and the amplitude of the phase current, respectively, $\varphi_{EN}$ is the phase corresponding to the back EMF harmonic of $N$th harmonic.

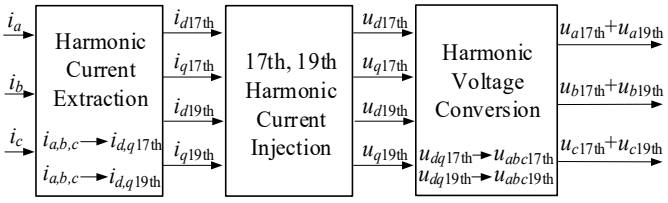


Fig. 13. Principle of harmonic current injection.

The torques of the proposed model before and after the harmonic current injection is compared in Fig. 14. Compared with the torque ripple of the proposed model, the torque ripple of the injected model is reduced to 17.04%, while the torque of the injected model is only reduced by 0.004Nm. The comparison of the torque harmonics is shown in Fig. 15, which means that 18th torque harmonic of the proposed model is greatly reduced, thus highly reducing the torque ripple.

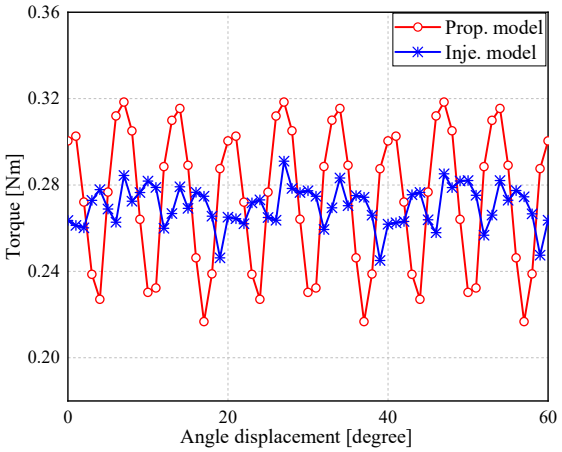


Fig. 14. The output torque waveform before and after injection.

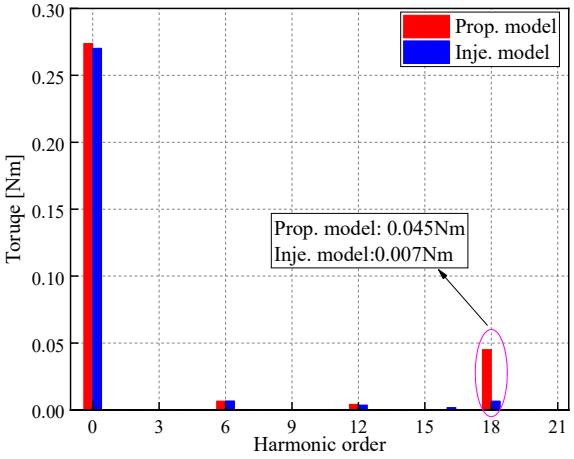


Fig. 15. The output torque harmonic before and after injection.

### D. Torque Characteristic Analysis

The asymmetric design of the rotor of the proposed model leads to the asymmetry of the air gap flux density and the flux offset, which will further affect the torque output performance at different current angles.

Fig. 16 shows the output torque of the proposed model at different current phase angles in one cycle. As can be seen from Fig. 16, if the proposed model produces a positive acceleration based on a given speed, the maximum torque can reach 0.274Nm during acceleration. And if the proposed model produces deceleration motion on the basis of a given speed, the maximum torque can only reach 0.171Nm during deceleration. The asymmetric torque problem during the acceleration and deceleration of the proposed model needs to be paid attention to in the debugging.

### E. PM Demagnetization Analysis

Since the PMs of the model are arranged in polymagnetic arrangement, there may be demagnetization risk affecting the

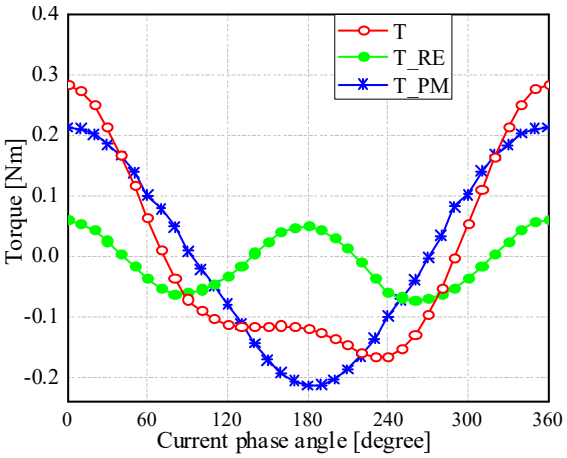


Fig. 16. Output torque of the proposed model at different current phase angles.

stability of the motor, so the demagnetization performance of the PMs of the motor is analyzed. The analysis of magnet demagnetization is carried out by analyzing the change of the magnet remanence before and after the current excitations. A ratio is defined as [28]:

$$\delta = (1 - \frac{B_r'}{B_r}) \times 100\% \tag{11}$$

where $B_r'$ is remanence of the magnet after a large stater current and $B_r$ is the initial remanence of the magnet.

The demagnetization rate of the proposed model under different currents is shown in Fig.17. In the maximum 6 times of rated current operation, the PMs of the motor have almost no demagnetization. This means that the proposed model has good anti-demagnetization performance and can run stably under operating conditions.

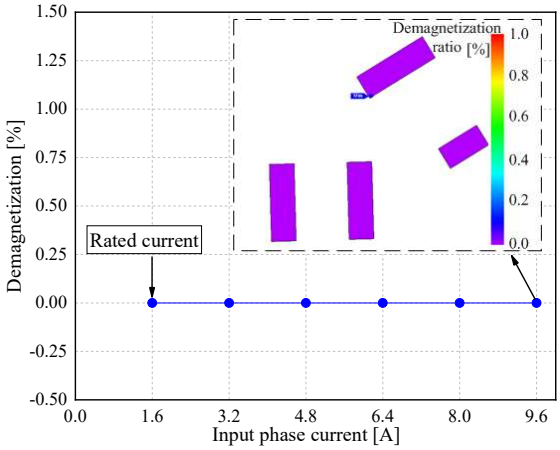


Fig. 17. Demagnetization analysis of the prop model.

## IV. Conclusion

This paper has proposed a novel PMA-SynRM with flux focusing effects to obtain high performance using an asymmetric rotor. The position-biased magnets with flux barrier design has been adopted for asymmetric rotor to not only focus the magnetic flux for high magnetic torque, but also increase the torque by making the magnetic and reluctance torques obtain the peak value at the same current phase angle. The specific conclusions are as follows:

1) The width of the side barrier $w$ sensitively affects the flux

focusing effects and motor performance. The peak torque of the proposed model is gained at $w$ = 1.1 mm, and the current phase angle is 0 degrees.

2) The output torque of the proposed model is increased by 28.04%, and the efficiency is increased by about 0.85% when compared with the basic model.

3) To reduce the 18th torque harmonic in the proposed model, a method of injecting the 17th and 19th harmonic current is adopted, and the torque ripple has been reduced from 35.9% to 17.04%.

4) The rotor Mises stress and PM demagnetization analysis confirm that the proposed model has good reliability for applications.

## REFERENCES


[1] I. Boldea, L. N. Tutelea, L. Parsa and D. Dorrell, "Automotive Electric Propulsion Systems With Reduced or No Permanent Magnets: An Overview," *IEEE Trans. Ind. Electron.*, vol. 61, no. 10, pp. 5696-5711, Oct. 2014.

[2] M. Zeraoulia, M. E. H. Benbouzid and D. Diallo, "Electric Motor Drive Selection Issues for HEV Propulsion Systems: A Comparative Study," *IEEE Trans. Veh. Technol.*, vol. 55, no. 6, pp. 1756-1764, Nov. 2006.

[3] H. Hwang, S. Bae and C. Lee, "Analysis and Design of a Hybrid Rare-Earth-Free Permanent Magnet Reluctance Machine by Frozen Permeability Method," *IEEE Trans Magn*, vol. 52, no. 7, pp. 1-4, July 2016, Art no. 8106304.

[4] M. Barcaro, N. Bianchi and F. Magnussen, "Permanent-Magnet Optimization in Permanent-Magnet-Assisted Synchronous Reluctance Motor for a Wide Constant-Power Speed Range," *IEEE Trans. Ind. Electron.*, vol. 59, no. 6, pp. 2495-2502, June 2012.

[5] H. Cai, B. Guan and L. Xu, "Low-Cost Ferrite PM-Assisted Synchronous Reluctance Machine for Electric Vehicles," *IEEE Trans. Ind. Electron.*, vol. 61, no. 10, pp. 5741-5748, Oct. 2014.

[6] S. Ooi, S. Morimoto, M. Sanada and Y. Inoue, "Performance Evaluation of a High-Power-Density PMASynRM With Ferrite Magnets," *IEEE Trans. Ind. Appl.*, vol. 49, no. 3, pp. 1308-1315, May-June 2013.

[7] M. Ibrahim, L. Masisi and P. Pillay, "Design of Variable-Flux Permanent-Magnet Machines Using Alnico Magnets," in IEEE Transactions on Industry Applications, vol. 51, no. 6, pp. 4482-4491, Nov.-Dec. 2015.

[8] I. Petrov and J. Pyrhonen, "Performance of Low-Cost Permanent Magnet Material in PM Synchronous Machines," *IEEE Trans. Ind. Electron.*, vol. 60, no. 6, pp. 2131-2138, June 2013.

[9] I. Boldea, L. N. Tutelea, L. Parsa, and D. Dorrell, "Automotive Electric Propulsion Systems with Reduced or No Permanent Magnets: An Overview," *IEEE Trans. Ind. Electron.*, vol. 61, no. 10, pp. 5696-5711, Oct. 2014.

[10] E. Trancho *et al*., "PM-Assisted Synchronous Reluctance Machine Flux Weakening Control for EV and HEV Applications," *IEEE Trans. Ind. Electron.*, vol. 65, no. 4, pp. 2986-2995, April 2018.

[11] Y. Kong, M. Lin and L. Jia, "A Novel High Power Density Permanent-Magnet Synchronous Machine With Wide Speed Range," *IEEE Trans Magn*, vol. 56, no. 2, pp. 1-6, Feb. 2020, Art no. 7505206.

[12] G. Xu, G. Liu, W. Zhao, Q. Chen and X. Du, "Principle of Torque-Angle Approaching in a Hybrid Rotor Permanent-Magnet Motor," *IEEE Trans. Ind. Electron*, vol. 66, no. 4, pp. 2580-2591, April 2019.

[13] S. S. Maroufian and P. Pillay, "Design and Analysis of a Novel PM-Assisted Synchronous Reluctance Machine Topology with AlNiCo Magnets," *IEEE Trans. Ind. Appl.*, vol. 55, no. 5, pp. 4733-4742, Sept.-Oct. 2019.

[14] D. Ngo, M. Hsieh, and T. A. Huynh, "Torque Enhancement for a Novel Flux Intensifying PMa-SynRM Using Surface-Inset Permanent Magnet," *IEEE Trans. Magn.*, vol. 55, no. 7, pp. 1-8, July 2019, Art no. 8106108.

[15] E. Castagnaro, G. Bacco and N. Bianchi, "Impact of Geometry on the Rotor Iron Losses in Synchronous Reluctance Motors," *IEEE Trans. Ind. Appl.*, vol. 55, no. 6, pp. 5865-5872, Nov.-Dec. 2019.

[16] M. Ferrari, N. Bianchi, and E. Fornasiero, "Analysis of Rotor Saturation in Synchronous Reluctance and PM-Assisted Reluctance Motors," *IEEE IEEE Trans. Ind. Appl.*, vol. 51, no. 1, pp. 169-177, Jan.-Feb. 2015.

[17] W. Kim et al., "Optimal PM Design of PMA-SynRM for Wide Constant-Power Operation and Torque Ripple Reduction," *IEEE Trans. Magn.*, vol. 45, no. 10, pp. 4660-4663, Oct. 2009.

[18] T. A. Huynh and M. Hsieh, "Comparative Study of PM-Assisted SynRM and IPMSM on Constant Power Speed Range for EV Applications," *IEEE Trans. Magn.*, vol. 53, no. 11, pp. 1-6, Nov. 2017, Art no. 8211006.

[19] T. A. Huynh and M. Hsieh, "Irreversible Demagnetization Analysis for Multilayer Magnets of Permanent Magnet-Assisted Synchronous Reluctance Machines Considering Current Phase Angle," *IEEE Trans. Magn*, vol. 55, no. 7, pp. 1-9, July 2019, Art no. 8106609.

[20] R. Moghaddam and F. Gyllensten, "Novel High-Performance SynRM Design Method: An Easy Approach for A Complicated Rotor Topology," *IEEE Trans. Ind. Electron.*, vol. 61, no. 9, pp. 5058-5065, Sept. 2014.

[21] D. -H. Jung, Y. Kwak, J. Lee and C. -S. Jin, "Study on the Optimal Design of PMa-SynRM Loading Ratio for Achievement of Ultrapremium Efficiency," *IEEE Trans. Magn.*, vol. 53, no. 6, pp. 1-4, June 2017, Art no. 8001904.

[22] W. Zhao, D. Chen, T. A. Lipo, and B. Kwon, "Performance Improvement of Ferrite-Assisted Synchronous Reluctance Machines Using Asymmetrical Rotor Configurations," *IEEE Trans. Magn.*, vol. 51, no. 11, pp. 1-4, Nov. 2015, Art no. 8108504.

[23] H. Yang, S. Lyu, H. Lin, Z. Zhu, H. Zheng and T. Wang, "A Novel Hybrid-Magnetic-Circuit Variable Flux Memory Machine," *IEEE Trans. Ind. Electron*, vol. 67, no. 7, pp. 5258-5268, July 2020.

[24] W. Zhao, H. Shen, T. A. Lipo, and X. Wang, "A New Hybrid Permanent Magnet Synchronous Reluctance Machine with Axially Sandwiched Magnets for Performance Improvement," *IEEE Trans. Energy Convers.*, vol. 33, no. 4, pp. 2018-2029, Dec. 2018.

[25] Y. Kong, M. Lin, M. Yin and L. Hao. "Rotor Structure on Reducing Demagnetization of Magnet and Torque Ripple in a PMa-synRM With Ferrite Permanent Magnet,". *IEEE Trans. Magn*, vol. 54, no. 11, pp. 1-5, Nov. 2018, Art no. 8108705.

[26] G. Chu, R. Dutta, M. F. Rahman, H. Lovatt, and B. Sarlioglu, "Analytical Calculation of Maximum Mechanical Stress on the Rotor of Interior Permanent-Magnet Synchronous Machines," *IEEE Trans. Ind. Appl.*, vol. 56, no. 2, pp. 1321-1331, March-April 2020.

[27] B. Lee, Z. Q. Zhu, and L. R. Huang, "Torque Ripple Reduction for 6-Stator/4-Rotor-Pole Variable Flux Reluctance Machines by Using Harmonic Field Current Injection," *IEEE Trans. Ind. Appl.*, vol. 53, no. 4, pp. 3730-3737, July-Aug. 2017.

[28] K. Wang, J. Li, S. S. Zhu, and C. Liu, "Novel Hybrid-Pole Rotors for Consequent-Pole PM Machines Without Unipolar Leakage Flux," *IEEE Trans. Ind. Electron.*, vol. 66, no. 9, pp. 6811-6823, Sept. 2019.


**Chengwu Diao** was born in China on April 1995. He received the B.S. degree and M.E degree in electrical engineering from Shenyang University of Technology, Shenyang, China, in 2018 and 2021. He is currently working toward the Ph.D. degree in the School of Electrical Engineering, Shandong University, Jinan, China.

His current research interests include design, analysis and control of electrical machines.

**Wenliang Zhao** (S'14–M'16) was born in China on May 1987. He received the B.S. degree in control science and engineering from Harbin Institute of Technology, China, in 2011, and the Ph.D. degree in electronic systems engineering from Hanyang University, South Korea, in 2015.

From 2015 to 2016, he was a Postdoctoral Fellow with Hanyang University, South Korea. In 2016, he joined the School of Electrical Engineering, Shandong University, as a Research Professor. Since 2020, he has been a Full Professor of Shandong University. He has authored or coauthored more than 100 papers on the topics of his research interests, which include design, analysis and control of electrical machines and power transformers.

**Yan Liu** was born in China on November 1994. He received the B.S. degree from China University of Mining and Technology, Xuzhou, China, in 2018, and M.E degree from Shandong University, Jinan, China, in 2021. He is currently working in China Aviation Control System Research Institute, mainly engaged in the field of motor design.

**Xiuhe Wang** was born in China on July 1967. He received the B.E. and M.E. degrees from Shandong University, Jinan, China, in 1989 and 1993, respectively, and the PhD degree from Shenyang University of Technology, Shenyang, China, in 1996.

From 2001 to 2002, he was a Postdoctoral Fellow with Seoul National University, Seoul, South Korea. He is currently a Professor of electrical engineering and the Vice Head of the School of Electrical Engineering, Shandong University. His research interests include permanent magnet machines, energy-efficient machines, theoretical analysis and calculation of electromagnetic devices, and their application on electrical machines. He has authored/co-authored more than 100 papers on these topics.